

High-Average-Power Laser Program
Optics and Chamber Studies:
Report on Research Performed During FY02

M. S. Tillack, F. Najmabadi and A. R. Raffray

October 1, 2003



**Fusion Division
Center for Energy Research**

University of California, San Diego
La Jolla, CA 92093-0417

ABSTRACT

This report describes the results of research performed at UC San Diego in support of the High Average Power laser program. Our research focuses on the prediction of chamber and optic response in inertial fusion energy (IFE) power plants and simulation of those phenomena through modeling and scaled experiments. Progress occurred in three primary topical areas: (1) Laser-induced damage to grazing-incidence metal mirrors, (2) IFE chamber dynamics and clearing following target explosions, and (3) Chamber wall materials response to pulsed loading by x-rays and high-energy ions.

Outline

1. Task 1: Final Optic Damage Studies
 - 1.1. Statement of purpose
 - 1.2. Background
 - 1.3. Progress in FY02
2. Task 2: Chamber Dynamics & Clearing
 - 2.1. Statement of Purpose
 - 2.2. Background
 - 2.3. Progress in FY02
3. Task 3: Experimental studies of laser-IFE chamber wall
 - 3.1. Statement of Purpose
 - 3.2. Background
 - 3.3. Progress in FY02

1. Task 1: Final Optic Damage Studies

1.1. Statement of purpose

Our research seeks to develop a better understanding of damage mechanisms and to demonstrate acceptable performance of grazing incidence metal mirrors (GIMM's), with an emphasis on the most critical concerns for laser IFE. Through both experimentation and modeling we will demonstrate the limitations on the operation of reflective optics for IFE chambers under prototypical environmental conditions. In addition, we will work together with other HAPL organizations to develop specific final optic design concepts for a laser-IFE power plant and to field both small and medium scale prototypes for testing. The top level goals for final optics in Phase I are:

1. Meet laser induced damage threshold (LIDT) requirements of more than 5 Joules/cm², in large area optics.
2. Develop a credible final optics design that is resistant to degradation from neutrons, x-rays, gamma rays, debris, contamination, and energetic ions.

We are concentrating on grazing incidence aluminum mirrors, as this has shown the most promise for a wider range of wavelengths. Our top level plans include the following three activities:

1. We will quantify the effects of various threats. The full range of damage threats in a laser-IFE power plant includes laser damage, contamination (dust, aerosol and condensate), x-rays, neutrons, and ions. Our work at UC San Diego will concentrate on laser-induced damage, including the effects of damage and contaminants on the LIDT. The work will include supporting modeling, with an emphasis on effects of mirror distortion on the wave front fidelity. We will investigate prototypical designs (*e.g.*, Al-coated SiC) and conditions (*e.g.*, vacuum and non-oxidizing environments), and will investigate the effects of larger area laser spot sizes in collaboration with NRL. We expect to have the effects of all the relevant threats quantified by late FY 2003/early FY 2004.
2. We will develop mitigation techniques for those threats that are found to be serious. These techniques include gas puffs, mechanical shutters, and magnetic diversion, depending on the threat. We do not expect to start these activities until after the threats have been quantified. This will probably be in FY 2004, with the needed mitigation schemes identified and evaluated by the end of FY 2005.
3. We will investigate fabrication techniques and integration issues. This includes bonding a thin aluminum coating to a neutron transparent substrate, developing environmental coatings resistant to contamination, exploring surface pre- and re-conditioning techniques and scale-up issues. We expect to establish a reference mirror fabrication technique by late FY 2003. In addition, we will begin to develop the techniques necessary to couple the final optic to the target tracking system in order to demonstrate our ability to steer beams and hit targets on the fly while maintaining acceptable beam characteristics.

1.2. Background

In any laser fusion system, the final optic for each beam is located in the direct line of sight of the exploding fusion targets. Consequently, that optic is exposed to a variety of damage threats. These include prompt neutron and gamma fluxes, x-ray and ionic emissions, and "long" time-scale threats from condensable target and chamber materials, as well as hydrodynamic pressure loads. The potential consequences include increased laser absorption, degradation of the beam quality, and reductions in the laser-induced damage threshold (LIDT).

Three primary goals for damage resistance have been specified previously [1]. We require that the optics operate for 2 years ($\sim 10^8$ shots) at an incident fluence level of 5 J/cm^2 (normal to the beam). In-situ reconditioning is allowed if it can be accomplished without significantly degrading the plant availability. The maximum tolerable level of damage corresponds with 1% increased absorption and degradation of the wavefront by $\lambda/3$ ($\lambda=248 \text{ nm}$ for KrF). An increase in absorption equivalent to 1% of the incident beam is likely to result in laser-induced damage to the optic as well as degradation of the spatial profile and increased difficulty balancing the power amongst many beams. The wavefront degradation limit was chosen based on two important target illumination constraints: the spatial nonuniformity of the beam on target must be less than 1% and the spot size and position must be known to within 20 microns. As a rule of thumb, surface aberrations of the order of $\lambda/3$ will lead to a doubling of the propagation parameter M [2], which corresponds to a doubling of the diffraction-limited spot size and a doubling of the beam divergence. The allowable wavefront distortion in the final optic depends on the allocation of wavefront distortions throughout the entire optical path as well as the margin for error. Pending further detail on the precise wavefront requirements on target, we are using $\lambda/3$ as our goal.

Figure 1. shows a design of a GIMM that uses a stiff low-activation substrate (such as C or SiC composite) and a thin aluminum coating on the surface [3]. Table 1 summarizes the R&D needs that were identified as important in order to establish the feasibility of this option. In our first two years of research, we concentrated on the basic optical behavior and damage mechanisms. In the next 3 years we propose to fill in the database for damage limits, develop and test more prototypical mirrors and also begin addressing engineering development and system integration.

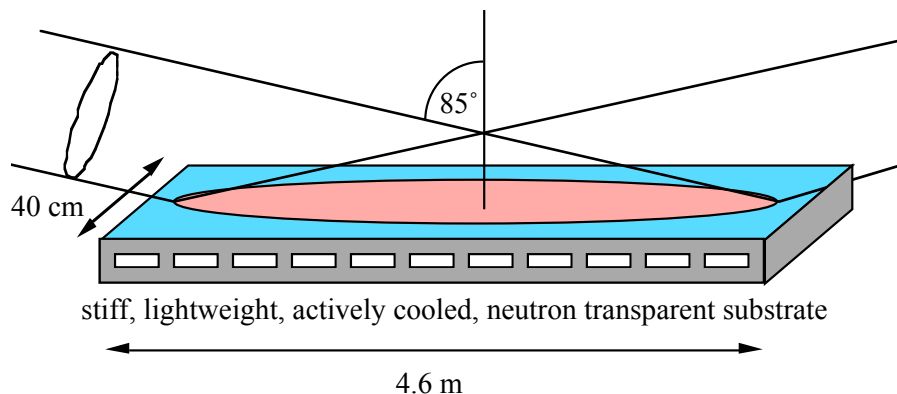


Figure 1.1. Diagram of a grazing-incidence mirror for an IFE power plant

Table 1. Key issues for grazing incidence mirrors in IFE [4]

1. Experimental verification of laser damage thresholds
 2. Experiments with irradiated mirrors
 3. Protection against debris and x-rays (shutters, gas jets, *etc.*)
 4. In-situ cleaning techniques
 5. Wavefront issues: beam smoothness, uniformity, shaping
 6. Large-scale manufacturing
 7. Cooling
-

1.3. Progress in FY02

During the past 2 years we have obtained both diamond-turned and Al-coated optics, and characterized the surfaces both before and after exposure using a variety of surface analysis techniques. Optics were obtained on an “as available” basis while we began to develop supplies of custom optics specifically designed to operate in a laser-IFE chamber environment. We have developed intimate contacts with SBIR contractors and are now engaged in a thorough exploration of optics suppliers in order to ensure that the HAPL program will be able to maintain a reliable supply of high-quality optics in the future.

We acquired a database of fluence limits for both 532 and 248 nm light at relevant fluences and pulse widths. Initial data at 532 nm showed very high damage resistance. For single shot exposures we were able to approach the melting point of Al – a fundamental limit of the material. For high shot count we obtained data which appeared to exceed the yield strength of Al. Damage levels as high as 40 J/cm² were obtained.

We installed a 0.4-J KrF laser together with associated optics and diagnostics. This gives us easier access to the desired wavelength and also provides a far more uniform spatial intensity profile without external manipulations. Testing at 248 nm resulted in far lower damage threshold. Surfaces survive for long periods of time above 5 J/cm² (which is our goal), but poor optic quality has hampered our ability to specify fluence limits with certainty.

To date we have not observed a “grazing angle instability”. Prior to testing, it was feared that small defects with a larger angle of incidence than the surface average would couple to the laser more strongly, possibly growing the defect in an unstable way. This was anticipated due to the strong angular dependence of the reflectivity of s-polarized light. On the contrary, we have observed a tendency for the laser to remove such defects. The creation of microscale roughness is observed, but the morphology tends to be aligned with the beam so as to avoid changes in the local angle of incidence.

Damage morphology has been observed with both 532 and 248 nm light. Large differences exist for these two wavelengths, both in the apparent mechanisms of damage as well as the damage threshold. UV light is more damaging due to the shorter wavelength and higher photon energy, and more interactive with the background environment. Therefore we plan to perform all future tests at 248 nm.

Due to observations of chemical reactions at the surface, in 2002 we assembled a vacuum cell for initial optics damage testing. Screening tests were performed and the results showed very significant changes in damage morphology as compared with tests in air. Therefore, we are planning to build a larger, more flexible vacuum chamber with better diagnostic access and base pressure of 1-2 mTorr.

During the past 2 years we have been actively seeking to develop modeling capabilities that will enable us to examine all of the anticipated surface defects that might occur. As shown in [Table 2](#), this includes both dimensional defects and compositional defects. The nature of the damage and the method of analysis depends most strongly on the size of the defect relative to the wavelength and whether the defect is embedded or attached. As we developed modeling capabilities, we applied them to examine test cases of interest which would help clarify the limits of damage. Modeling is proceeding step-by-step together with experiments.

During the past two years we have made progress modeling dimensional defects and gross surface contamination [5]. At present we are concentrating our development effort on methods to analyze localized composition defects (see Table 2).

Table 2. Modeling techniques used to analyze the effects of defects on laser propagation

Dimensional Defects		Compositional Defects		
□>□, Gross deformations	□<□, Surface morphology	Gross surface contamination	Local defects: external contaminants	Local defects: internal species
Modeling techniques used or under development:				
Optical design software (ZEMAX)	Kirchhoff scattering theory	Full-wave multi-layer Fresnel model	Mueller matrix (image theory)	Model of refractive index variations

2. Task 2: Chamber Dynamics & Clearing

2.1. Statement of Purpose

Our research aims at developing a fully integrated computer code to simulate and study the dynamic behavior of IFE chamber, including: the hydrodynamics; the effects of various heat sources and transfer mechanisms such as photon and ion heat deposition and chamber gas conduction, convection, and radiation; the chamber wall response and lifetime; and the cavity clearing.

2.2. Background

In a rep-rated laser-fusion facility, the pulse repetition rate is limited by the time it takes for chamber environment to return to a sufficiently quiescent and clean low-pressure state following a target explosion to allow a second shot to be initiated. Laser propagation and beam quality on the target as well target injection and tracking are impacted by the number density, temperature, mix of chamber constituents as well as fluid eddies and turbulence in the chamber.

Many physical phenomena with different time scale occur in the chamber following the target implosion. In the “fast” time scale, X-rays, ions and neutrons from the target implosion travel through the chamber. Depending on the chamber constituents, the X-rays and ions can interact and deposit part of their energy in the chamber. The remaining portion of X-rays and ions arrive at the chamber wall where they deposit their energy. For the case of wetted walls, the wetting agent vaporizes and enters the chamber. In the case of a dry wall protection scheme, photons and ions will interact and affect the surface wall materials in different ways that could result in the emission of atomic (sublimation or vaporization) and macroscopic particles, thereby limiting the lifetime of the wall. Also, mass loss in the form of macroscopic particles can be much larger than mass loss due to the surface vaporization. The “fast” time scale which covers this “first pass” of target X-rays and ions through the chamber can take up to a few microseconds. At the end of this phase, the chamber environment is in a non-equilibrium phase (*e.g.*, non-uniform pressure) and a new source of material is introduced in the chamber.

After this “fast” time scale phase, the chamber environment evolves more slowly, mainly in the hydrodynamics time scale. The aim of the proposed research is to understand the chamber evolution and dynamic over this “longer” time scale and investigate the constraints imposed by chamber dynamics on the laser driver rep-rate.

The focus of our research effort is the development of a fully integrated computer code to model and study the chamber dynamic behavior, including: the hydrodynamics; the effects of various heat sources and transfer mechanisms such as photon and ion heat deposition and chamber gas conduction, convection, and radiation; the chamber wall response and lifetime; and the cavity clearing. Since developing such a simulation capability is a major undertaking, the development of this simulation code is envisioned in several steps of increasing sophistication, *i.e.*, the code will be developed in a modular fashion such that it can be readily and easily upgraded and more detailed physics modules added. In this fashion, the code itself can be used through its

development to set priorities -- simple models can be added as modules to the code to assess the importance of different processes under different conditions. In addition, utilization of developed expertise in computational fluid dynamics allows us to focus mostly on developing and understanding relevant phenomena. Within these criteria, two years ago we proposed a three-year activity in development of a chamber dynamics clearing code. Code development was broken into separate stages, each taking roughly one year of research

Stage 1 (2001 proposal): Develop the core including the input/output interfaces, the geometry definition and the numerical solution control for transient hydrodynamics (2-D transient compressible Navier Stokes equations). Simple models for radiation and heat transport will be included. Results from BUCKY will be used as initial conditions. Boundary conditions are included through “wall-interaction” modules.

Stage 2 (2002 proposal): Develop a detailed radiation transport package. Improve on “wall-interaction” modules based on analysis performed with stage 1 code. Implement adaptive mesh routines if necessary & extend the capability of the code to 2-D geometries with arbitrary shape.

Progress in Stage 1 and 2 code development is described in the next section (Sec. 2.3). The simulation code, SPARTAN, is fully functional and initial simulation results are described below. We have met all milestones to date. We propose to use SPARTAN in this period to simulate dynamic behavior of laser-IFE chambers and to incorporate models of additional physical phenomena.

2.3. Progress in FY02

We have developed the SPARTAN simulation code. The code solves 2-D transient compressible Navier Stokes equations. Consistent with our goal of utilizing existing computational fluid dynamics capabilities and based on discussions with several specialists in the field, the code utilizes a state-of-the-art CGF solver package (after Colella, Glaz, and Ferguson) that is based on a second-order shock-capturing Godunov scheme [6,7]. It consists of a robust algorithm for compressible Euler equations and is second-order accurate in regions of smooth flow capturing shocks with a minimum of numerical dissipation and overshoot. CGF algorithm was modified to account for dissipative terms such as viscosity.

An early version of SPARTAN (stage 1 code) was completed over 1 year ago. It became apparent rapidly that in order to accurately capture the dynamic behavior of chamber over a long period of time, a high density spatial grid has to be used to account for moving structures such as shocks and eddies. As a result, a typical run time of SPARTAN over the time of period of interest (100 ms) would take a couple of weeks on a high-end personal computer. We, therefore, proceeded with introducing adaptive mesh refinement (AMR) algorithm in SPARTAN. The algorithm used in this work was presented by Almgren *et al.* in [8]. This algorithm automatically places high density ground around the moving shock and eddy structure while using a low-density grid elsewhere. Basically, the solution grid is organized into levels from coarse to fine. The AME algorithm tags each region based on density and energy gradients and the grid and decide if a coarser or finer grid is appropriate and proceeds accordingly until the desired level of grid is achieved. The AMR algorithm also interpolates the solution both in space and time

between the grid levels. This AMR technique has been quite successful in reducing the run time of SPARTAN from a couple of weeks to several hours.

Another important change introduced in SPARTAN last year was the capability to model arbitrary two-dimensional geometry. Our simulations with early versions of SPARTAN highlighted that the geometry of the chamber wall have a dramatic impact on the evolution of chamber environment on the slow time scale. Current version of SPARTAN can handle arbitrary two-dimensional geometry using an embedded boundary technique developed by Modiano *et al.* [9]. We have started using SPARTAN to model the dynamic behavior of IFE chambers. Some simulation results are given below. These simulations have also highlighted and prioritized the physical phenomena that should be included in later version of SPARTAN.

The simulation results below are made for a cylindrical chamber with a radius of 6.5 m. One laser beam tube with a length of 20 m and diameter of 1 m is included to demonstrate the capability of the code to model arbitrary geometry (see Fig. 2.1). The initial conditions are taken from the BUCKY one-dimensional rad-hydro code 500 μ s after the target explosion. At this time, the initial shock wave from the target explosion has not arrived at the wall so that chamber geometry does not affect the solution. The one-dimensional BUCKY solution is rotated symmetrically around target explosion point and used as the initial condition. In addition, at this time (500 μ s after the target explosion), the chamber gas is cooled enough such that chamber gas is transparent to radiation and, therefore, there is no need to include detailed radiation transport models (see Section 2.4 for more discussion).

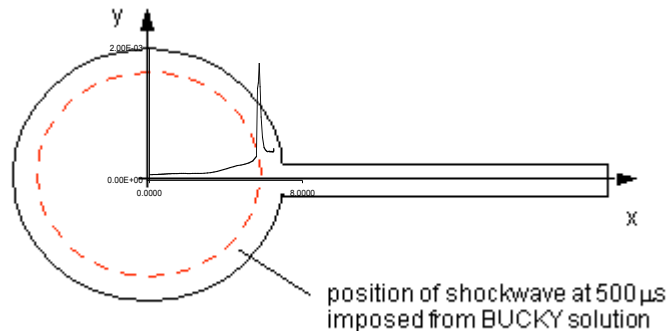


Fig. 2.1. Physical model of simulation domain including the initial condition from BUCKY.

Figure 2.2 shows a detailed view of color-coded chamber gas pressure contours at the entrance of the laser beam channel shortly after the initial shock wave intersect the chamber wall. The figure shows a reflected shock wave with a structure developed because of the presence of the beam channel. The solution grid is superimposed on this figure to demonstrate the AMR algorithm in action. This figure shows that even relatively small structure on the wall geometry causes dramatic impact on the structure of reflected shocks in the chamber

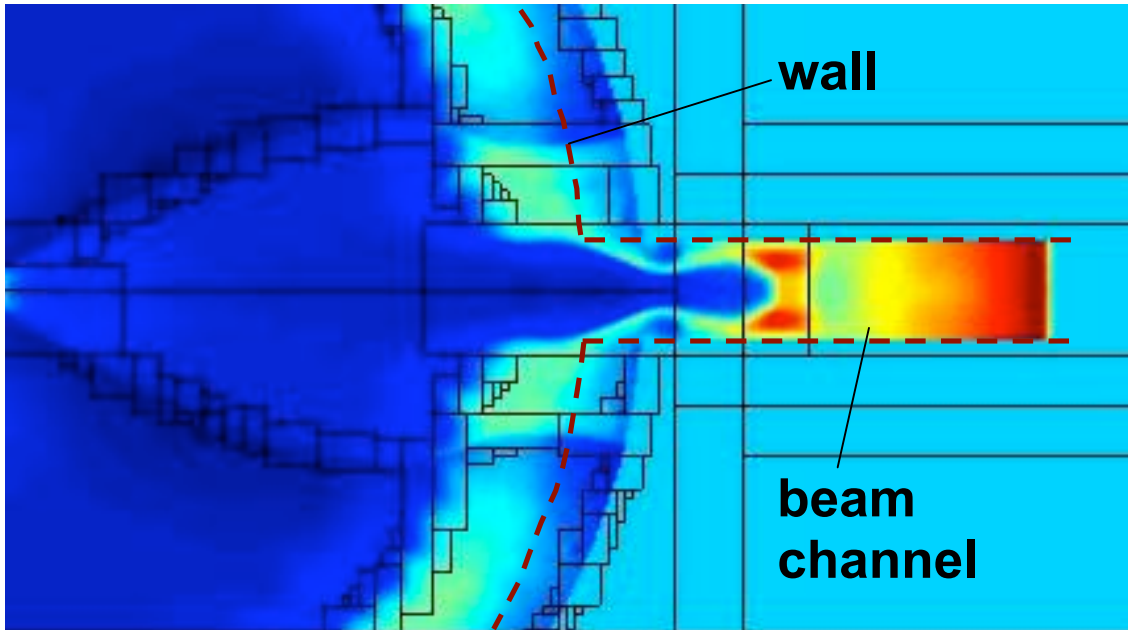


Figure 2.2 Color-coded chamber gas pressure contours at the entrance of the laser beam channel shortly after the initial shock wave intersect the chamber wall. The solution grid is superimposed on this figure to demonstrate the AMR algorithm in action.

Figure 2.3 shows color coded pressure and temperature contours in the chamber 100 ms following the target explosion. Significant eddy structure can be seen in the chamber gas. This simulation corresponds to the case when the target is exactly at the center of the chamber. We have found that the exact location of target at the time of explosion does not affect the chamber environment at long time intervals.

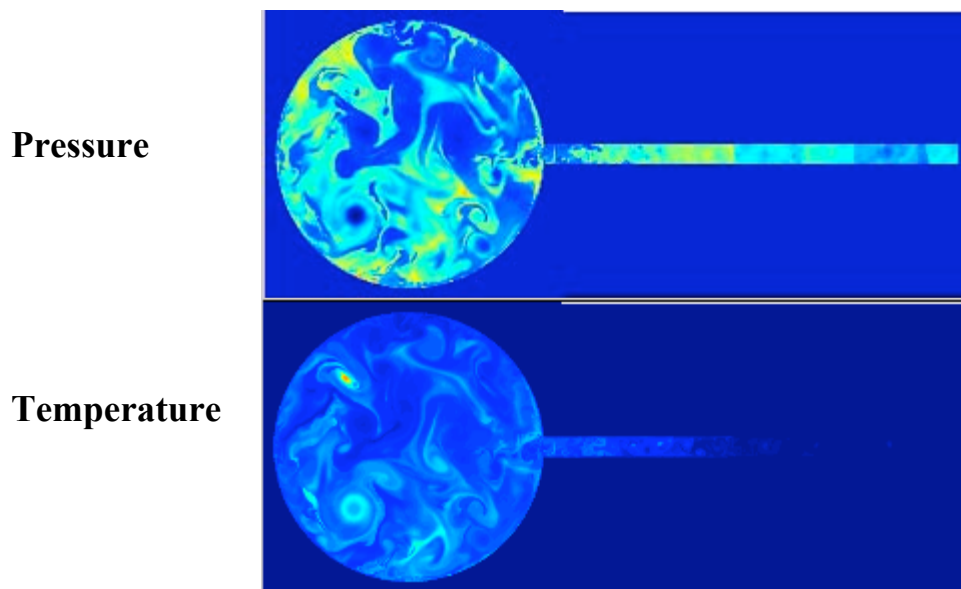


Figure 2.3. Color coded pressure and temperature contours in the chamber 100 ms following the target explosion. Significant eddy structure can be seen in the chamber gas.

The impact of shock waves from target explosion on final optics has been a major concern. Figure 2.4 shows the pressure on a final optics mirror located at the end of beam channel. It is assumed the mirror is normal to beam tube and there is no opening in the beam channel to deflect the pressure wave. As such this calculation is probably conservative by an order of magnitude. The result shows that pressure on the mirror is so small that mechanical forces of the mirror are negligible.

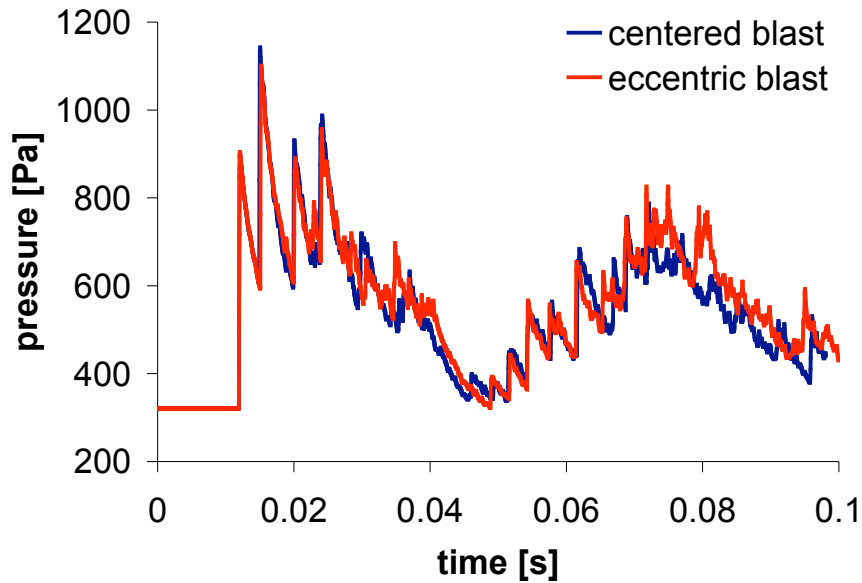


Figure 2.4. Pressure at the final optics (mirrors) as a function of time following the target explosion. The structure in the pressure profile is due to the reflection of initial shock in the main chamber.

The SPARTAN code is now ready for release to the laser-IFE community. Two journal papers on this research are in preparation.

INEEL Tasks (PI: J. Phil Sharpe)

Over the past year INEEL has worked to add models of aerosol nucleation and growth, allowing simulation of particulate effects on chamber engineering issues. The basic computational structure for aerosol calculations in the code allows the addition of mechanisms impacting particulate dynamics in an IFE system. Items to be added include charged-particle induced nucleation and growth, carbon particulate generation, and how subsequent target explosions effect particulate accumulation. INEEL will continue to contribute to the development of SPARTAN through the following tasks:

Year 1: Task 1: Develop and incorporate a model to simulate carbon particulate formation (the physical properties of carbon preclude application of standard growth models)

Year 2: Task 1: Investigate the effect of charged species remaining in the afterglow plasma on aerosol nucleation and growth; add mechanisms to the aerosol module

Task 2: Investigate methods and/or existing nucleation data relevant to IFE chamber conditions for use in validating nucleation models

Year 3: Task 1: Begin development to extend the module to multi-component aerosol dynamics, allowing simulation mixed material interaction in the IFE chamber

Task 2: Test chamber clearing code against existing data and/or methods

3. Task 3: Experimental studies of laser-IFE chamber wall

3.1. Statement of Purpose

Our research aims at developing and testing candidate material for the wall of laser-IFE chambers that can accommodate the laser IFE threat spectra and provide the required lifetime.

3.2. Background

Predictive capability of the IFE chamber response requires a detailed understanding of the response of the chamber wall as the wall response dictates the constituents of the laser IFE chamber:

1. Properties of the chamber buffer gas (*e.g.*, type and density) are dictated by the survivability of the chamber wall,
2. Material ejected from the wall represent a major portion of material in the chamber

Most of the research previously has focused on wall mass loss due to sublimation. For a given x-ray and ion flux on the wall, temperature evolution of the wall is computed for perfectly flat wall using steady state and bulk properties for pure material. Mass loss is then estimated based on sublimation and/or melting correlations. These analyses indicate that the temperature variation mainly occurs in a thin region ($<100 \mu\text{m}$) and large temperature gradients are limited to first few (or ten) microns. Beyond this region, the first wall experiences a much more uniform heat flux. As such, we proposed two years ago to use a thin armor instead of a monolithic chamber wall. Armor can then be optimized to handle rapid particle and heat flux while the first wall is optimized for structural function and efficient heat removal at quasi-steady-state. In addition, in an IFE power plant, most of the neutrons are deposited in the back where blanket and coolant temperature will be at quasi steady state due to thermal capacity effect. As such, most first-wall and blanket concepts developed for MFE will be directly applicable to IFE applications. There are several possibilities for armor material: 1) W and other refractory metals, 2) Carbon (and CFC composites), and 3) more exotic engineered material. Each has its own set of potential advantages and critical issues that should be addressed with rigorous R&D. In particular, means for in-situ repair of the armor should receive special attention.

There are a large number of uncertainties associated with the armor:

A. Material loss due to increased wall temperature (*e.g.*, evaporation, sublimation)

1. Surface features in a practical system are typically larger than tens of microns and impurities and contaminants can cause hot spots. As such, wall temperature estimates are highly uncertain.
2. Sublimation is extremely sensitive to material temperature and partial pressure. Accurate knowledge of wall temperature is essential in sublimation estimates. Steady-state data for sublimation rates may not be applicable to fast transients in the chamber wall. Sublimation at local hot spots (contaminants, surface morphology) may dominate. Indirect material loss due to contaminants on the surface may be important. Examples include formation of WC on

the wall which has a melting point much lower than W or formation of CH on the wall that can vaporizes at very low temperature.**B. Failure due to Thermomechanical loads**

1. Rapid differential thermal expansion caused by thermal shock can cause catastrophic failures of armor and back wall.
2. Rep-rated thermal expansion and resulting stresses can lead to armor failure due to thermal fatigue.
3. The joint between armor and back wall can fail due to rep-rated thermal expansion and fatigue.
4. It is possible that significant material loss does not occur for metallic armors even if a small layer of armor melts during each shot. Melting and solidification of this melt layer may have adverse (loss of strength) or positive (removal of defects) in thermomechanical response of the armor.
5. Contaminants and impurities can impact the armor response to any of the above mechanisms.

C. Material loss due to ion and neutron bombardment

1. Neutron irradiation affects the thermophysical properties of the armor material. While full resolution of this issue awaits construction of intense 14~MeV neutron source (corresponding to expected fusion neutron spectrum from the exploding target), some insight is gained through test in fission reactors.
2. Sever ion bombardment of the armor material could lead to massive material loss. For example, implantation of He ions in particular in W (in which He diffusion is very poor) can result in a 1 to 1 ratio of W to He within about 100 days of operation assuming a 1 μ m implantation depth. This would lead to sever blistering of armor and must be remedied by solutions such as operation at high enough temperature for He to be mobile in W or by using very fine porous structure providing a very short diffusion path for He to be transported to open porosity and back to the chamber. The above experimental observations are for mono-energetic ions in which all ions come to rest at the same location in the material. The ions arriving at the IFF chamber wall have a range of energies and, therefore, calculations show that this issue may not be a large concern. Experiments are needed to confirm this theoretical prediction.

As a source with integrated and prototypical spectrum of x-rays and ions is not available, experiments should be performed in simulation facilities. Our analysis indicates that most of phenomena leading to the failure of the wall depend on wall temperature evolution (temporal and spatial) and chamber environment; only sputtering and radiation (ion & neutron) damage effects depend on “how” the energy is delivered. Several means for delivering energy in ns time-scale are available: lasers, x-ray sources, electron beams, and ion beams. Lasers provide a “clean” source of energy for wall simulation experiments. Irradiation of wall samples with lasers does not impose any constraint on the experimental chamber and, thus, make is relatively easy to field diagnostics. We have shown that a 10-ns laser pulse can simulate temperature evolution in the wall sample that is prototypical of laser IFE chambers response to x-rays (see [Figure 3.1](#)). Peak wall temperature and temperature gradients in the wall can be easily adjusted by controlling the laser energy and/or modification of laser pulse shape. In addition, relatively low-cost laser system can produce sufficient rep-rate to easily investigate wall response to 10^6 shots. This is especially an attractive option as existing YAG laser at UCSD can be used for this purpose.

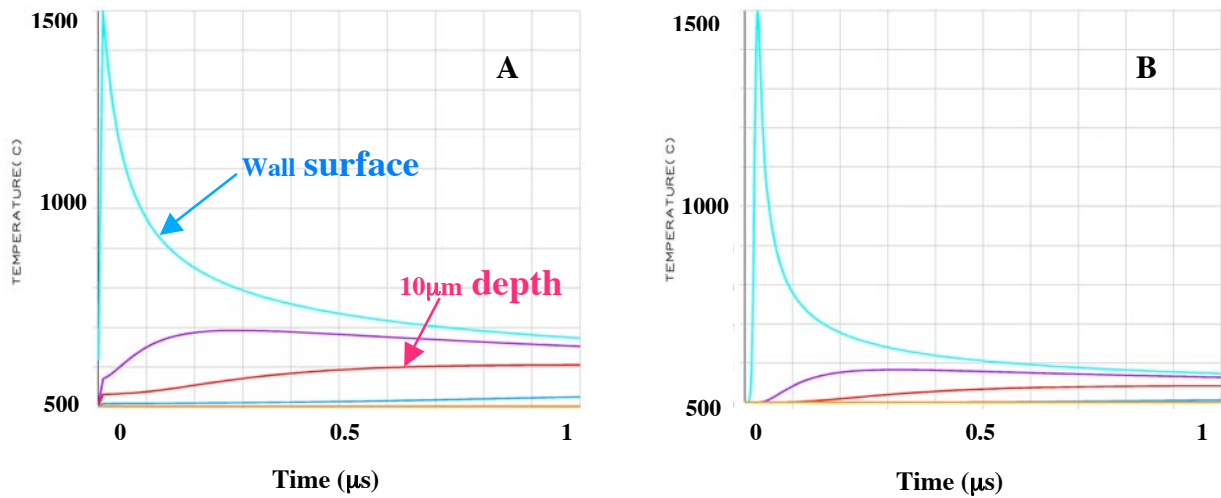


Figure 3.1. Temperature history in a tungsten flat wall subjected to a) NRL direct-drive target x-ray channel and b) a 10 ns Gaussian laser pulse. Temperature evaluation on the surface and at depths of 5, 10, and 20 microns are shown. Only the laser energy is adjusted such that similar peak wall temperature (~1500 C) is achieved in the simulation experiments.

Ion sources are considerably more expensive but they would provide additional data, as the primary energy release channel in direct-drive capsules is the ion channel. The existing RHEPP facility at Sandia has been used to study wall response. The drawback of this facility is its low rep-rate and the fact that ion spectrum is not similar to that expected from an IFE target explosion. In addition, special diagnostics has to be fielded on RHEPP to measure temperature evolution of sample in real time. Overall, our conclusion is that laser provides the most flexible and low-cost option to investigate laser-IFE chamber wall response. Similar simulation experiments (but at low rep-rate, with small number of shots, and smaller suite of diagnostics) can be fielded in RHEPP facility. The combination of two efforts provides a large body of experimental database for laser-IFE wall research. In particular, comparison of experimental results from a laser facility with similar experiments performed in RHEPP will underline if the wall failure mechanism is mainly due to temperature evolution and/or other effects can be important.

3.3. Progress in FY02

Under Grant from Naval Research Laboratory last year, we designed and built a simulation experimental facility to determine thermo-mechanical response of the chamber wall. An illustration of the experimental set-up is shown in Figure 3.2. The energy source is our existing 2 J (at 1 micron) Nd-YAG laser. It can operate at 10-HZ allowing rep-rated experiments (10^6 shots per day), if necessary. Our laser includes injection seeding for reproducible and smooth temporal profiles. We have utilized an existing vacuum chamber with inside dimensions of 10"x12". Our vacuum system is capable of pressures below 10^{-8} torr and includes a gas feed system to inject a mixture of four types of gases in the chamber to simulate chamber

environment and contaminants. Experimental set up is mounted on an optical breadboard and placed in the chamber.

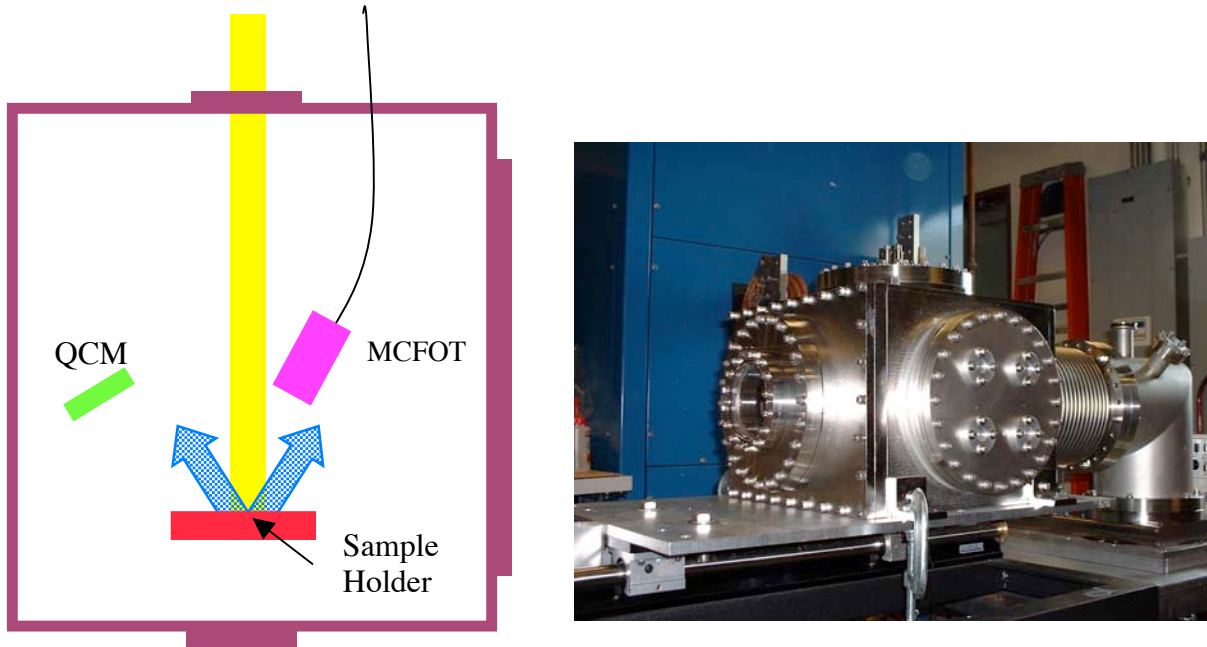


Figure 3.2. Schematic of simulation experiments of the chamber wall. The existing vacuum vessel is also shown.

The thermomechanical response of the armor depends strongly on the equilibrium temperature of the armor between shots. For IFE chambers, equilibrium wall temperature ranges from 600 to over 1000 °C. During last year we designed, built and fielded a high-temperature sample holder which can maintain the equilibrium sample temperature from room temperature to 1,200 °C. This sample holder operating at 1,000 °C is shown in [Fig. 3.3](#). Endurance runs of several runs at 1,200 °C have been performed to demonstrate the reliability of the sample holder.

In order to correlate experimental results with computations and develop a predictive capability, accurate measurement of sample temperature evolution during the shot is necessary (nanosecond resolution). We have developed a fast optical thermometer with nanosecond resolution. This thermometer is based on multi-color optical thermometry technique. Published work on multi-color optical thermometry were limited to response time of millisecond to micro-second. In addition, they include complicated optical trains that would be difficult to implement in the experimental chamber. We have used fiber optics technology to simplify the optical train and used high speed photo-multiplier tubes and scopes in order to achieve the necessary speed. [Figure 3.4](#) through [3.6](#) shows that the details of our optical thermometer. We have calibrated our thermometer using the Optronics UL-45U lamp with a total error of < 1.5%.

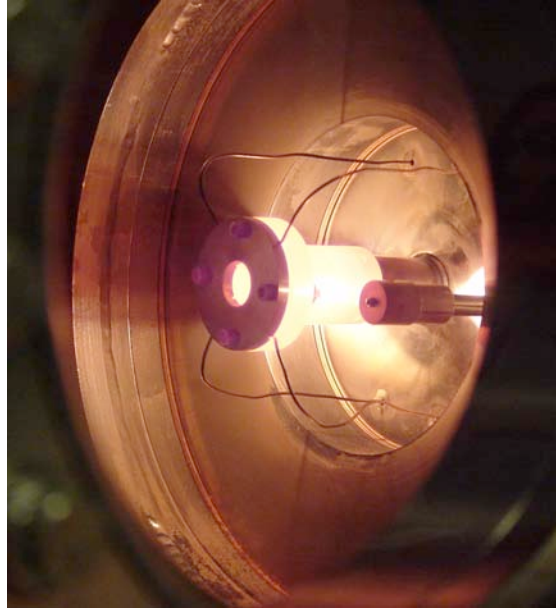


Figure 3.3. Photograph of sample holder operating at 1,000 °C inside the experiment chamber.

The electric signal from the photo-multiplier tube is measured using fast scopes (1 GHz, up to 5 GS/s). A PC downloads the data from the scope through internet and does the necessary data analysis and displays the temperature evolution. In addition, we have installed a master timing control system with ~100 ps jitter allows operation from single shot up to 10 Hz. At present, we are performing initial experiments with the assembled system. During the next two month we will also install quartz micro-balancing and RGA diagnostics on the chamber to measure material loss from the sample in situ and in real time. Production runs will be performed as soon as samples are obtained from Oak Ridge National laboratory.

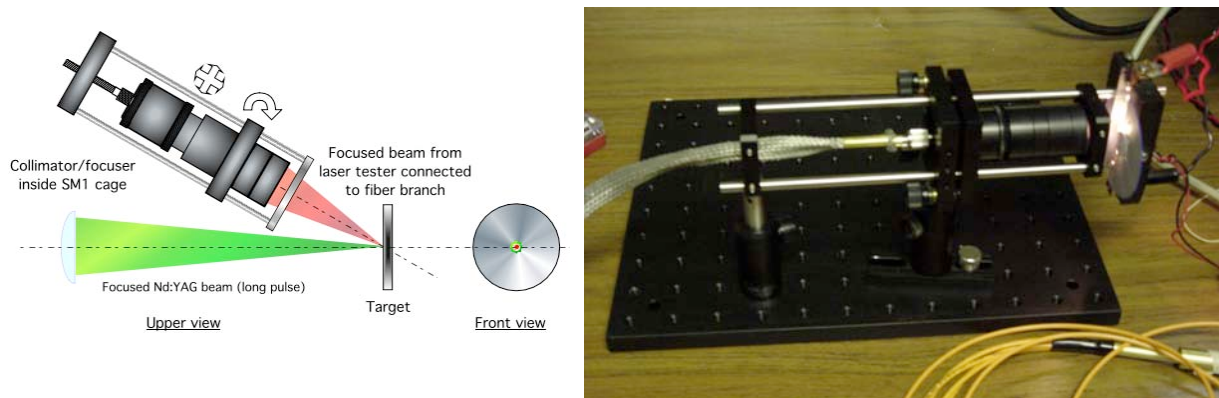


Figure 3.4. Sensor head of the optical thermometer. The rugged design with accurate swivel and tilt control allows sensor head to be focused to < 1 mm² spots with a high degree of position accuracy. Thermal radiation from the spot is injected by the sensor head into four bundled low-OH silica fibers.

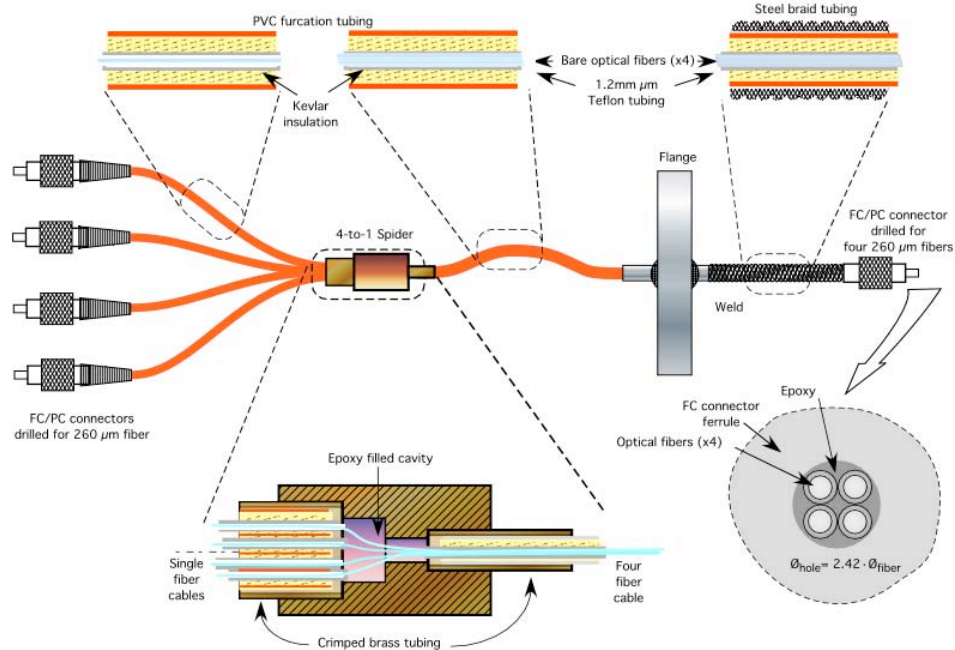


Figure 3.5. Fiber optics relay connects the sensor head to collimator focuser element of photo-multiplier tubes. One of the fiber optics lines is used by a positing laser that allows the sensor head to be pointed on the desired sport on the sample.

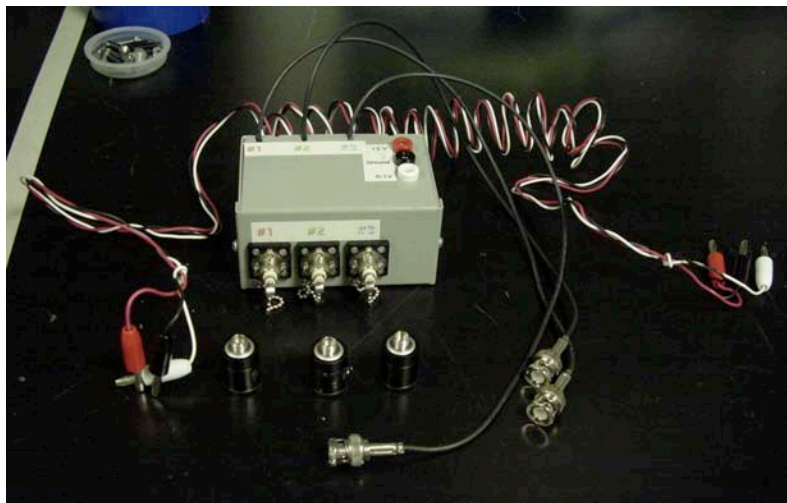


Figure 3.6. The light signal in each optical fiber is focused by a collimator focuser onto a photo-multiplier tube. Three photo-multiplier tubes are mounted in the box shown above. The collimator/focuser elements are also shown.

References:

1. M. S. Tillack, S. A. Payne, N. M. Ghoniem, M. R. Zaghoul and J. F. Latkowski, "Damage threats and response of final optics for laser-fusion power plants", 2nd Int. Symp. on Inertial Fusion Science and Applications, Kyoto Japan, Sept. 2001.
<http://aries.ucsd.edu/LIB/REPORT/CONF/IFSA01/tillack.pdf>
2. C. D. Orth, S. A. Payne, and W. F. Krupke, "A Diode Pumped Solid State Laser Driver for Inertial Fusion Energy," *Nuclear Fusion* 36 (1996) 75-116.
3. L. M. Waganer, "Innovation Leads the Way to Attractive IFE Reactors – Prometheus-L & Prometheus-H," IAEA Technical Committee Meeting and Workshop on Fusion Reactor Design and Technology, 13-17 Sept. 1993.
4. R. L. Bieri and M. W. Guinan, "Grazing Incidence Metal Mirrors as the Final Elements in a Laser Driver for Inertial Confinement Fusion," *Fusion Technology* 19 (May 1991) 673-678.
5. T. K. Mau, M. S. Tillack, and M. R. Zaghoul, "Modeling of Mirror Surface Damage Effects on Beam Propagation in a Laser-Driven IFE Power Plant", 19th IEEE/NPSS SOFE, Atlantic City NJ, Jan. 21-25, 2002.
<http://aries.ucsd.edu/LIB/REPORT/CONF/SOFE01/mau.pdf>
6. G. H. Miller and E. G. Puckett "A high-order Godunov method for multiple condensed phases," *J. Comput. Phys.* **128** (1996) 134.
7. Marcus Day, Center for Computational Sciences and Engineering at Lawrence Berkeley National Laboratory, private communications.
8. Almgren, A. S., Bell, J. B., Colella, P., Howell, L. H. 1993 "An adaptive projection method for the incompressible Euler equations," in Proceedings of the 11th AIAA Computational Fluid Dynamics Conference in Orlando, Florida, July 6-9, 1993.
9. D. Modiano and P. Colella: "A higher-order embedded boundary method for time-dependent simulation of hyperbolic conservation laws", Proceedings of FEDSM'00, 2000.